Observation of Quantum Tunneling between Two Plasmonic Nanoparticles

Jonathan A. Scholl,*[†] Aitzol García-Etxarri,[†] Ai Leen Koh,[‡] and Jennifer A. Dionne*[†]

[†]Department of Materials Science and Engineering, Stanford University, Stanford, California 94305, United States
[‡]Stanford Nanocharacterization Laboratory, Stanford University, Stanford, California 94305, United States

S *Supporting Information*

ABSTRACT: The plasmon resonances of two closely spaced metallic particles have enabled applications including single-molecule sensing and spectroscopy, novel nanoantennas, molecular rulers, and nonlinear optical devices. In a classical electrodynamic context, the strength of such dimer plasmon resonances increases monotonically as the particle gap size decreases. In contrast, a quantum mechanical framework predicts that electron tunneling will strongly diminish the dimer plasmon strength for subnanometer-scale separations. Here, we directly observe the plasmon resonances of coupled metallic nanoparticles as their gap size is reduced to atomic dimensions. Using the electron beam of a scanning transmission electron microscope (STEM), we manipulate pairs of ∼10-nm-diameter spherical silver nanoparticles on a substrate, controlling their convergence and eventual coalescence into a single nanosphere. We simultaneously employ electron energy-loss spectroscopy (EELS) to observe the dynamic plasmonic properties of these dimers before and after particle contact. As separations are reduced from 7 nm, the dominant dipolar peak exhibits a redshift consistent with classical calculations. However, gaps smaller than ∼0.5 nm cause this mode to exhibit a reduced intensity consistent with quantum theories that incorporate electron tunneling. As the particles overlap, the bonding dipolar mode disappears and is replaced by a dipolar charge transfer mode. Our dynamic imaging, manipulation, and spectroscopy of nanostructures enables the first full spectral mapping of dimer plasmon evolution and may provide new avenues for in situ nanoassembly and analysis in the quantum regime.

KEYWORDS: Plasmonics, electron energy-loss spectroscopy, nanoparticle dimer, quantum tunneling
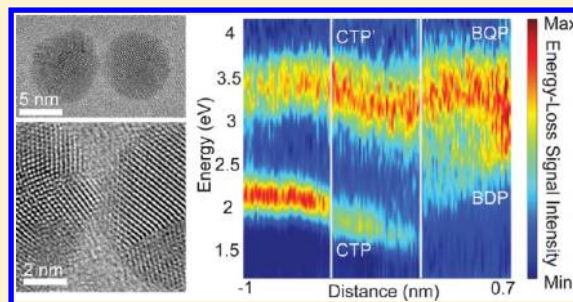
Electromagnetic radiation can interact strongly with metallic nanoparticles, exciting collective oscillations of conduction electrons known as localized surface plasmon resonances. In multiparticle systems, the plasmonic modes of individual particles hybridize to form new, collective modes.[1] Depending on the multiparticle geometry, these modes can exhibit enhanced or entirely distinct properties from the individual particle plasmons, ranging from strongly amplified near-field intensities[2,3] to Fano-like interference effects and emergent optical magnetism.[4]

Among the most geometrically simple but versatile multi-particle structures is the nanoparticle dimer. As two particles approach each other, bonding and antibonding modes emerge, corresponding to in-phase or out-of-phase interaction of individual particle plasmons.[1,5] Analogous with molecular orbital theory, the bonding mode exhibits a continual redshift in wavelength (i.e., reduced energy) and increased interparticle field intensity as particle separations are reduced. In contrast, the antibonding mode exhibits a slight blueshift with decreasing particle separation and a field node within the gap.

Nanoparticle dimers have been exploited in applications ranging from sensing and spectroscopy[1,6,7] to nonlinear optics,[8] but typically in a classical context. Indeed, for particle separations greater than ∼0.5 nm, classical local or nonlocal

electromagnetic models can be used to describe the dimer response, as confirmed through recent experiments.[9−11] But as particles come within very close proximity, quantum tunneling is expected to play an increasingly important role. Recent calculations indicate that electron tunneling between particles would increase the gap conductance, modifying the nature of the plasmonic modes.[3,12,13] These properties could be exploited to develop novel quantum plasmonic devices, such as tunable quantum optical antennas,[14] optical rectifiers,[15] or optical scanning tunneling microscopes.

Thus far, however, accessing plasmonic modes in the quantum tunneling regime has proven challenging. Fabricating and characterizing very small interparticle separations (sub-0.5-nm) is difficult even with state-of-the-art lithography[9,16] and self-assembly.[10,11,17,18] An added complication is correlating the precise dimer geometry with its plasmonic response. An ideal study would involve the direct observation and in situ spectral analysis of individual particle dimers that could be manipulated in real-time to vary their interparticle separation from classical down to quantum scales.
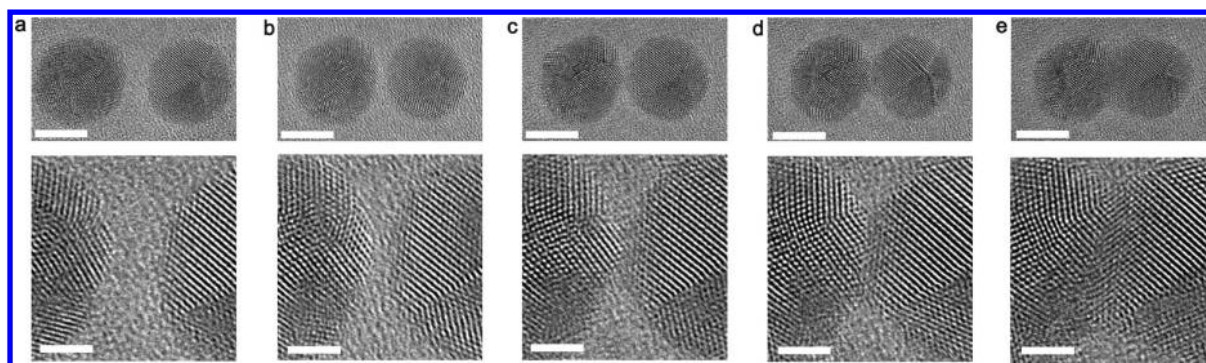
Figure 1. Aberration-corrected TEM images of a silver nanosphere dimer, with particles converging and coalescing under the influence of the electron beam. The particles are 9 nm in diameter and supported on an 8-nm-thick SiO_2 membrane substrate. The electron beam induces particle convergence from an edge-to-edge separation of 2 nm (a) down to 1 nm (b) and 0.35 nm (c). The energy of the beam also allows the particles to coalesce and recrystallize once in contact. Negative values of separation (or overlaps) of −0.5 nm (d) and −1 nm (e) are shown. Scale bars in the top and bottom rows equal 5 and 2 nm, respectively.
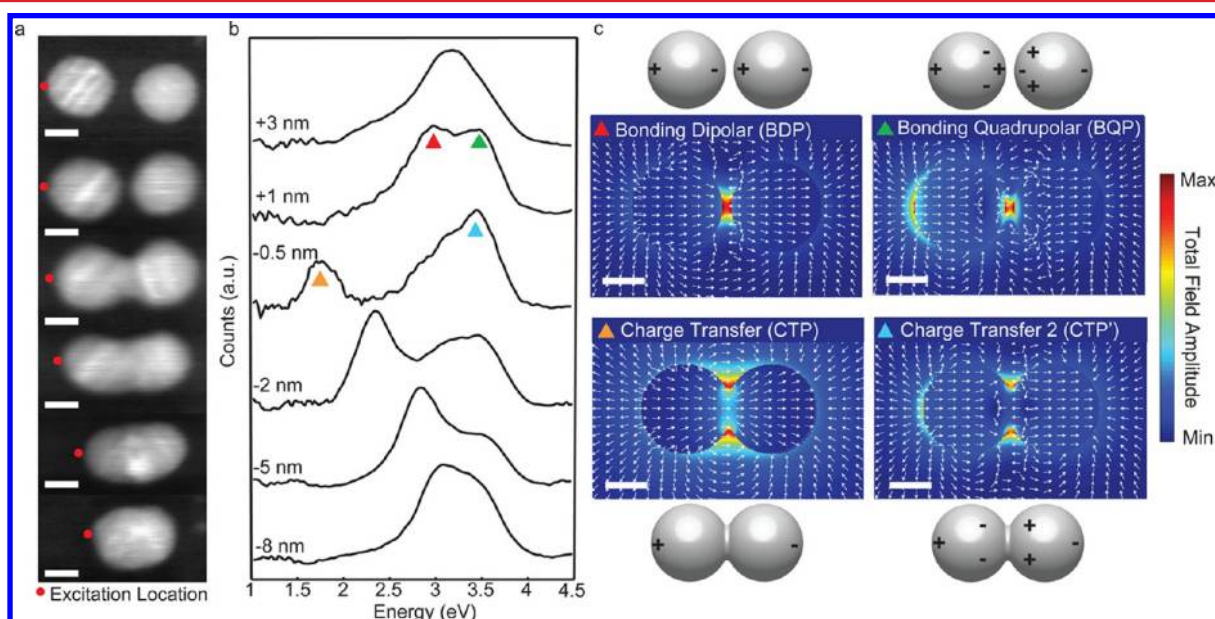

Figure 2. STEM images of a merging dimer, correlated with experimental plasmonic spectra and theoretical field profiles. A homodimer of 10-nm-diameter spheres controllably coalesces with a STEM beam placed 1 nm from the particle edge. STEM images (a) are matched with their corresponding electron energy-loss spectra (b) at various separation distances from +3 to −8 nm. Depending on the system geometry, certain plasmonic modes are allowed and disallowed. Illustrations of the particle polarization and BEM-generated total field amplitude maps of the four main contributing modes are included, with arrows indicating field directions (c). All scale bars equal 5 nm.

In this Letter, we use the electron beam of a transmission electron microscope (TEM) to spatially manipulate individual, ∼10-nm-diameter silver nanosphere dimers. The electron beam induces motion of the particles along a substrate, allowing controlled convergence and coalescence of particles. We simultaneously perform electron energy-loss spectroscopy to monitor the plasmonic response of the system. This method allows the correlation of spectra with the dimer geometry, including gap dimensions and particle shape and size. Our results provide the first conclusive experimental confirmation of recent quantum plasmon theories,[3,13] while introducing a new experimental technique for simultaneous nanomanipulation and analysis in the quantum regime.[19]

We investigate silver nanoparticles due to their strong electric polarizability; this property results in plasmonic resonances with narrow spectral linewidths and intense coupling at small gap sizes, yielding identifiable spectral shifts. The nanospheres are colloidally synthesized without organic ligands to eliminate

molecular-damping effects on the resonances[21] and enable full dimer particle convergence to a single, larger nanoparticle. Briefly, aqueous silver nitrate is reduced to silver nanospheres using sodium borohydride as both the reducing agent and the electrostatic stabilizer in solution.[22,23] The synthesized particles are deposited on an 8-nm-thick SiO_2 membrane TEM substrate, a smooth, inert surface that facilitates particle movement.

Particle imaging, manipulation, and electron energy-loss spectroscopy (EELS) signal collection are accomplished using an aberration-corrected FEI Titan TEM operated at 300 keV with an imaging resolution of 0.07 nm (0.27 nm in STEM mode). The electron microscope instigates particle convergence and coalescence in both TEM and STEM modes through the focusing of the electron beam to a small area on the sample. As described by others, the motion may be caused by electron beam-facilitated surface diffusion of the nanoparticles' atomic constituents[24−27] and nanoparticle polarization due to the

passing electron's electric field.[28,29] If the polarizations of the individual particles of a dimer become aligned, an attractive Coulombic force can be generated between them. In our experiments, the electron beam is used to induce convergence and coalescence of silver nanoparticles as large as 20 nm.

High-resolution aberration-corrected TEM images of a homodimer of 9-nm-diameter silver nanospheres, with particles converging and coalescing, are shown in Figure 1. The particles begin from a separation of approximately 2 nm (Figure 1a) and are translated into closer proximity by the electron beam (Figure 1b and c). As the particles contact, a few atom wide bridge forms (Figure 1d) and broadens (Figure 1e), demonstrating an expanding twin plane across the junction. The surface diffusion instigated by the electron beam[24−27] results in a recrystallization and reshaping of the cluster into an ellipse and, ultimately, a single, thermodynamically-stable sphere.

From a nanomaterials perspective, these results agree well with recent studies of in situ TEM of platinum nanoparticle growth in a liquid cell.[30] Electron-beam catalyzed growth of platinum nanoparticles illustrates similar twinning events and surface diffusion toward the neck region. Since our study uses substantially larger particles (up to 20 nm diameters versus 1 nm for Pt), we can achieve considerably slower and more controllable particle aggregation. This slow convergence of particles is essential to map the classical-to-quantum plasmon transition.

Using STEM-EELS, we can simultaneously observe the plasmonic resonance evolution as the particles of the dimer merge. Compared to TEM, STEM techniques have the advantage of selectively exciting certain plasmonic modes based on the beam placement.[9,21,31] In our study, we direct the probe 1 nm outside the edge of the dimer, along the longitudinal axis, to excite the bonding plasmon mode[32] that can be directly compared with optical studies of dimers.[33] The rate of particle approach is tunable by the electron-beam intensity. Using a 0.1 nA current, we can controllably translate 9−11 nm diameter particles at an average velocity of approximately 0.02 nm/s. This slow rate is essential to observe particle separations of less than 0.5 nm (approximately two Ag atomic planes), where electron tunneling effects should appear.

Figure 2a illustrates STEM snapshots of the motion of a 10-nm-diameter silver homodimer, from a 3 nm separation to full particle coalescence. These 10 nm particles are large enough to generate sufficient EELS signal without any intrinsic size-dependent effects[21] while also sufficiently small to be controllably moved. Figure 2 also includes the corresponding EEL spectra of the plasmonic modes at select stages of particle motion.

We first investigate plasmon resonances in the classical realm. Figure 2b includes experimental EELS data for particle separations of +3, +1, −0.5, −2, −5, and −8 nm. Negative separation distances correspond to overlapping particles. As described below, a number of spectral resonances between 1 and 4.5 eV can be observed. To identify the physical character of these modes, we use the boundary element method (BEM).[34,35] BEM calculations simulate the response of the system to an electron beam incident 1 nm outside the edge of the dimer along its longitudinal axis. The simulations use empirical bulk dielectric functions[36] and assume hard spheres with a diameter of 10 nm in vacuum. In our calculations, the bridge connection between coalesced spheres is smoothed by

an arc of a 0.3 nm radius of curvature. Figure 2c plots the fields scattered by the modes at their simulated resonant frequencies.

At a gap size of +3 nm, the dimer experimental EELS data (Figure 2b) displays a bonding dipolar plasmon (BDP) resonance at 3.2 eV. BEM simulations indicate this mode is characterized by electon-beam-induced aligned dipoles in each particle with a large charge separation across the gap. Interparticle coupling causes this energy to be red-shifted from the resonance energy of an isolated particle at 3.35 eV. As the particles approach to within +1 nm, the experimental dipolar resonance continues to redshift to 3.0 eV, and a higher order resonance appears at 3.5 eV. BEM simulations identify this mode as a bonding quadrupolar plasmon (BQP), characterized by two second-order resonances on the individual particles, coupled by the gap.

After the particles have made contact, the gap-based bonding plasmonic modes are replaced with lower and higher-order charge transfer plasmon resonance modes (CTP and CTP′, respectively). These modes are characterized by the flow of electrons between the joined particles. As seen in the experimental EELS data for a separation of −0.5 nm, the CTP and CTP′ modes are observed at energies of 1.75 and 3.45 eV. The BEM CTP profiles of Figure 2c show how the entire conjoined particle now acts as a single dipole or multipole.

As the bridge between the two spheres broadens, the impedance of the particle connection evolves from capacitive to inductive in nature, causing a blueshift of the charge transfer modes.[7] Once the connection extends the full transverse diameter of the nanospheres, the aggregate has formed into an ellipse, and the resonant modes are dependent on the structure's aspect ratio. As seen in Figure 2a and b, a coalesced particle with dimensions of 13 × 10 nm is characterized by a lowest-order resonance at 3.1 eV. Continued electron-beam-induced coalescence of the particles ultimately results in formation of a single sphere of diameter ∼12 nm (data not shown), with a single resonance at 3.3 eV.

How do the bonding dipolar, quadrupolar, and charge transfer mode energies and intensities evolve with particle separation? The full, continuous trend of plasmonic mode shift and emergence is plotted in Figure 3. The particles range from essentially noninteracting at a separation of +8 nm to fully coalesced at −10 nm. The figure includes both theoretical spectra, calculated from a classical BEM model, and experimental data points corresponding to the EELS resonance peaks. The data points are determined from a combination of STEM images and EEL spectra of 20 individual spherical dimer pairs. We consider homodimers with particle diameters between 9 and 11 nm at various stages during their convergence and coalescence. The plasmon energies across this size range should theoretically only vary by <0.05 eV for a given separation, enabling comparison across all such homodimer pairs. A 95% confidence interval of ∼±0.1 eV for the resonance energy was determined through a statistical analysis of 10 spectral acquisitions associated with each STEM image collection. Note that the experimental data has been shifted by 0.15 eV, to account for substrate effects that are not modeled in the BEM theory (see Supporting Information).

Despite slight geometric variations during the coalescence events (e.g., atomic bridge formation), the experimental and BEM theoretical results demonstrate remarkable qualitative agreement over the classical size range (excluding subnanometer gaps). For example, the experimental peak energies
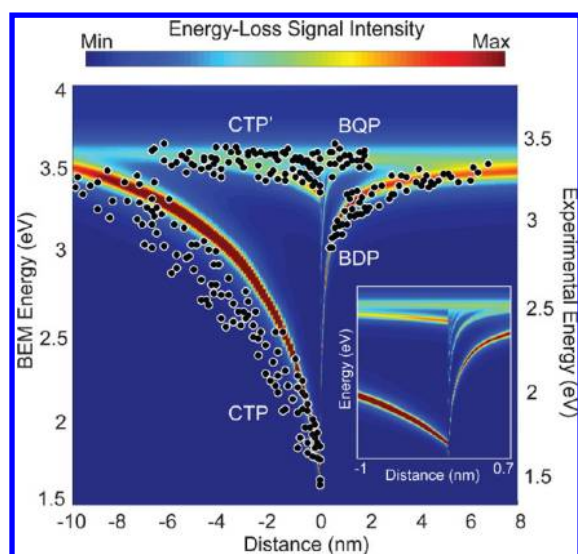
Figure 3. Comparison of classical BEM EELS calculations with experimental EELS resonances. BEM simulations consider a 10-nm-diameter nanosphere homodimer in vacuum with edge separation distances from +8 to −10 nm. The inset provides a zoom of the classically calculated resonances for distances between +0.7 and −1 nm. Data points represent experimental electron energy-loss spectral peaks correlated to STEM images from 20 individual dimer pairs at various stages of particle coalescence. The points have a spectral energy 95% confidence interval of ∼ ±0.1 eV. Note that the BEM and experimental axes are shifted by 0.15 eV to account for the plasmon energy redshift due to the substrate. Experimental data agree well with classical theory throughout the spatial range, with the exception of the quantum size regime (gaps < 0.5 nm).

accurately track the bonding dipolar and quadrupolar mode evolution predicted by BEM for separations larger than 0.5 nm. Also, after convergence, the charge transfer modes exhibit a

blueshift commensurate with BEM calculations. As described in the Supporting Information, most quantitative variations between the BEM predictions and experiments can be explained by substrate and geometric merging effects. However, as detailed below, we observe a distinct divergence of experimental plasmon peak data compared to the classical theory for separations smaller than 0.5 nm.

To investigate plasmon behavior in this subnanometer regime, we experimentally analyze the full spectral evolution of modes as dimers converged and coalesced. Figure 4a plots the EEL spectra of a 9-nm-diameter homodimer with an interparticle separation tuned from +0.7 to −1.0 nm. Note that separations between +0.7 and 0 nm correspond to less than three atomic lattice spacings of Ag (the close-packed lattice spacing is 0.24 nm).

To obtain this experimental data set, we use the STEM beam to induce particle motion at a rate of approximately 0.02 nm/s while simultaneously acquiring the particle's EELS data. Sets of 50 spectra are collected during continuous EELS acquisition, with STEM images obtained at the beginning and end of each scan, indicated by the solid vertical lines. Note that, because the electron beam in the imaging process can also induce a slight degree of particle motion, the boundary between each scan is not necessarily continuous.

When the particles are at separation distances greater than ∼0.5 nm, both the dipolar and the quadrupolar resonances are present in the experimental EEL spectra, similar to the classical theory. As the particles continue to approach, however, the experimental dipolar resonance intensity decreases and does not demonstrate the strong redshift predicted by the classical BEM model (Figure 3 inset). Interestingly, the experimental quadrupolar resonance does not diminish and retains its intensity until the particles are touching. Finally, upon particle contact, the charge transfer modes emerge, similar to classical theory.
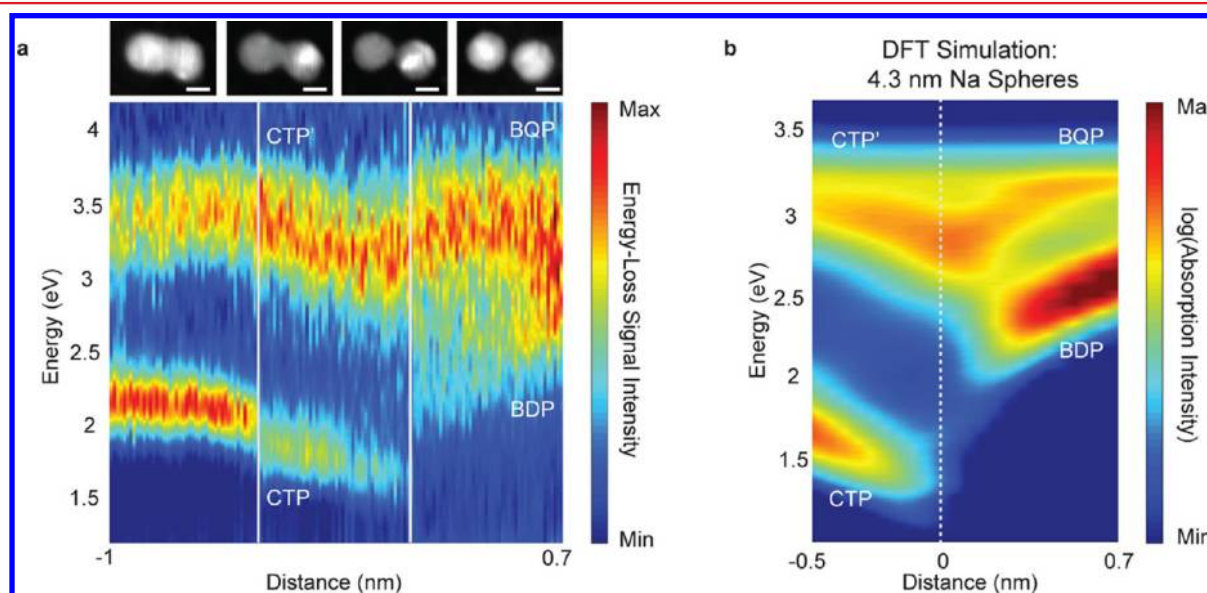

Figure 4. Continuous EELS collection to observe quantum tunneling effects at small gap sizes for silver spheres and theoretical comparison with sodium spheres. (a) A STEM-EELS probe enables particle motion during EEL spectra collection of a 9-nm-diameter silver homodimer. STEM images collected at the beginning and end of each scan (bounded by solid vertical lines) indicate the separation distances (+0.7, < 0.27, −0.3, and −1.0 nm). (b) DFT simulation of the plasmonic response of 4.3-nm-diameter sodium spheres in vacuum from recent work,[13] with particle separation between +0.7 and −0.5 nm. The spectra from both experiment and theory exhibit a diminished BDP resonance peak at separations of only a few angstroms, indicating quantum tunneling. The charge transfer mode appears after particle contact. Image scale bars equal 5 nm.

These experimental spectral observations and discrepancies with classical models have recently been predicted through ab initio density functional theory (DFT) calculations.[3,12,13] These quantum models incorporate the spill-out of electrons beyond the physical boundaries of the particles and the electron tunneling that is possible for small gap sizes. As metallic particles approach at distances less than ~0.5 nm, an increasing electron tunneling current neutralizes the charge separation at the junction between the spheres, reducing the built-up electric field and BDP resonance intensity.

Figure 4b depicts recent DFT calculations for the plasmonic response of 4.3-nm-diameter sodium spheres in vacuum.[13] Despite differences in material parameters (e.g., plasma frequency), the data show close qualitative correspondence to our experimental work, including the disappearance of the BDP mode prior to direct particle contact. Both experimental and quantum theoretical results are in contrast with classical models, which predict an increased BDP interparticle field intensity and a BDP resonance energy that approaches zero as the particles become separated by angstrom or sub-angstrom distances.[5,13]

The correspondence of our experimental results with quantum theory has several implications for future dimer-based applications. First, our findings indicate that interparticle separations smaller than ~0.5 nm exhibit lower-intensity bonding dipolar resonances and minimal additional resonance shifts compared to larger separations. This, in accordance with recent quantum theories,[3] implies that field enhancements will saturate around this separation—an important consideration for future plasmonic nanoantenna and sensor-based designs. Second, our results suggest that quantum tunnelling effects only become significant for interparticle separations of approximately two atomic lattice spacings. However, alternative plasmonic materials or configurations may afford additional flexibility for enhanced tunneling. Alternative particle geometries could also disentangle the effects of quantum tunnelling from nonlocality. For example, dimers of larger particles should demonstrate a more dramatic nonlocal response before entering the quantum tunneling regime. Finally, the direct observation of quantum tunneling implies that in situ assembly and analysis of new quantum plasmonic devices is possible. Ultimately, the ability to controllably manipulate and probe atomic-sized junctions may open new avenues for exploration, in fields ranging from quantum optics to molecular electronics.

ASSOCIATED CONTENT

Ⓢ Supporting Information

Further details about the nanoparticle synthesis, electron microscopy, and boundary element method simulations. This material is available free of charge via the Internet at http://pubs.acs.org.

AUTHOR INFORMATION

Corresponding Author
*E-mail: jdionne@stanford.edu; jscholl@stanford.edu.

Notes
The authors declare no competing financial interest.

ACKNOWLEDGMENTS

REFERENCES

(1) Halas, N. J.; Lal, S.; Chang, W.-S.; Link, S.; Nordlander, P. *Chem. Rev.* **2011**, *111*, 3913−61.

(2) García de Abajo, F. J. *J. Phys. Chem. C* **2008**, *112*, 17983−7.

(3) Marinica, D. C.; Kazansky, A. K.; Nordlander, P.; Aizpurua, J.; Borisov, A. G. *Nano Lett.* **2012**, *12*, 1333−9.

(4) Sheikholeslami, S. N.; García-Etxarri, A.; Dionne, J. A. *Nano Lett.* **2011**, *11*, 3927−34.

(5) Romero, I.; Aizpurua, J.; Bryant, G. W.; García de Abajo, F. J. *Opt. Express* **2006**, *14*, 9988−99.

(6) Stiles, P. L.; Dieringer, J. A.; Shah, N. C.; Van Duyne, R. P. *Annu. Rev. Anal. Chem.* **2008**, *1*, 601−26.

(7) Schnell, M.; García-Etxarri, A.; Huber, A. J.; Crozier, K.; Aizpurua, J.; Hillenbrand, R. *Nat. Photonics* **2009**, *3*, 287−91.

(8) Kim, S.; Jin, J.; Kim, Y.-J.; Park, I.-Y.; Kim, Y.; Kim, S.-W. *Nature* **2008**, *453*, 757−60.

(9) Duan, H.; Fernández-Domínguez, A. I.; Bosman, M.; Maier, S. A.; Yang, J. K. W. *Nano Lett.* **2012**, *12*, 1683−9.

(10) Yang, L.; Wang, H.; Yan, B.; Reinhard, B. M. *J. Phys. Chem. C* **2010**, *114*, 4901−4908.

(11) Ciracì, C.; Hill, R. T.; Mock, J. J.; Urzhumov, Y.; Fernández-Domínguez, A. I.; Maier, S. A.; Pendry, J. B.; Chilkoti, A.; Smith, D. R. *Science* **2012**, *337*, 1072−4.

(12) Zuloaga, J.; Prodan, E.; Nordlander, P. *Nano Lett.* **2009**, *9*, 887−91.

(13) Esteban, R.; Borisov, A. G.; Nordlander, P.; Aizpurua, J. *Nat. Commun.* **2012**, *3*, 825.

(14) Merlein, J.; Kahl, M.; Zuschlag, A.; Sell, A.; Halm, A.; Boneberg, J.; Leiderer, P.; Leitenstorfer, A.; Bratschitsch, R. *Nat. Photonics* **2008**, *2*, 230−3.

(15) Ward, D. R.; Hüser, F.; Pauly, F.; Cuevas, J. C.; Natelson, D. *Nat. Nanotechnol.* **2010**, *5*, 732−6.

(16) Jain, P. K.; El-Sayed, M. A. *Chem. Phys. Lett.* **2010**, *487*, 153−64.

(17) Lassiter, J. B.; Aizpurua, J.; Hernandez, L. I.; Brandl, D. W.; Romero, I.; Lal, S.; Hafner, J. H.; Nordlander, P.; Halas, N. J. *Nano Lett.* **2008**, *8*, 1212−8.

(18) Kern, J.; Großmann, S.; Tarakina, N. V.; Häckel, T.; Emmerling, M.; Kamp, M.; Huang, J.-S.; Biagioni, P.; Prangsma, J. C.; Hecht, B. *Nano Lett.* **2012**, *12*, 5504−9.

(19) During review of our manuscript, another group independently published experiments revealing the effects of electron tunneling on plasmon modes (ref 20). While the experimental methods are very distinct, the results exhibit excellent agreement.[20]

(20) Savage, K. J.; Hawkeye, M. M.; Esteban, R.; Borisov, A. G.; Aizpurua, J.; Baumberg, J. J. *Nature* **2012**, *491*, 574−577.

(21) Scholl, J. A.; Koh, A. L.; Dionne, J. A. *Nature* **2012**, *483*, 421−7.

(22) Creighton, J. A.; Blatchford, C. G.; Albrecht, M. G. *J. Chem. Soc., Faraday Trans. 2* **1979**, *75*, 790−798.

(23) Solomon, S. D.; Bahadory, M.; Jeyarajasingam, A. V.; Rutkowsky, S. A.; Boritz, C.; Mulfinger, L. *J. Chem. Educ.* **2007**, *84*, 322−325.

(24) José-Yacámán, M.; Gutierrez-Wing, C.; Miki, M.; Yang, D.-Q.; Piyakis, K. N.; Sacher, E. *J. Phys. Chem. B* **2005**, *109*, 9703−11.

(25) Chen, Y.; Palmer, R. E.; Wilcoxon, J. P. *Langmuir* **2006**, *22*, 2851−5.

(26) Lim, T. H.; McCarthy, D.; Hendy, S. C.; Stevens, K. J.; Brown, S. A.; Tilley, R. D. *ACS Nano* **2009**, *3*, 3809−13.

(27) Asoro, M. A.; Kovar, D.; Shao-Horn, Y.; Allard, L. F.; Ferreira, P. J. *Nanotechnology* **2010**, *21*, 025701.

(28) Reyes-Coronado, A.; Barrera, R. G.; Batson, P. E.; Echenique, P. M.; Rivacoba, A.; Aizpurua, J. *Phys. Rev. B* **2010**, *82*, 235429.

(29) Batson, P. E.; Reyes-Coronado, A.; Barrera, R. G.; Rivacoba, A.; Echenique, P. M.; Aizpurua, J. *Nano Lett.* **2011**, *11*, 3388−93.

(30) Yuk, J. M.; Park, J.; Ercius, P.; Kim, K.; Hellebusch, D. J.; Crommie, M. F.; Lee, J. Y.; Zettl, A.; Alivisatos, A. P. *Science* **2012**, *336*, 61−4.

(31) Nelayah, J.; Kociak, M.; Stéphan, O.; García de Abajo, F. J.; Tencé, M.; Henrard, L.; Taverna, D.; Pastoriza-Santos, I.; Liz-Marzán, L. M.; Colliex, C. *Nat. Phys.* **2007**, *3*, 348−353.

(32) Koh, A. L.; Bao, K.; Khan, I.; Smith, W. E.; Kothleitner, G.; Nordlander, P.; Maier, S. A.; Mccomb, D. W. *ACS Nano* **2009**, *3*, 3015−3022.

(33) García de Abajo, F. J. *Rev. Mod. Phys.* **2010**, *82*, 209−275.

(34) García de Abajo, F. J.; Howie, A. *Phys. Rev. Lett.* **1998**, *80*, 5180−5183.

(35) García de Abajo, F. J.; Howie, A. *Phys. Rev. B* **2002**, *65*, 115418.

(36) Johnson, P. B.; Christy, R. W. *Phys. Rev. B* **1972**, *6*, 4370−4379.